Systems/Circuits

Response of Neuronal Populations to Phase-Locked Stimulation: Model-Based Predictions and Validation

Nima Mirkhani,[1] Colin G. McNamara,[1,2] Gaspard Oliviers,[1] Andrew Sharott,[1] Benoit Duchet,[1] and Rafal Bogacz[1]

[1]MRC Brain Network Dynamics Unit, Nuffield Department of Clinical Neurosciences, University of Oxford, Oxford OX1 3TH, United Kingdom and [2]University College Cork, Cork T12 K8AF, Ireland

Modulation of neuronal oscillations holds promise for the treatment of neurological disorders. Nonetheless, conventional stimulation in a continuous open-loop manner can lead to side effects and suboptimal efficiency. Closed-loop strategies such as phase-locked stimulation aim to address these shortcomings by offering a more targeted modulation. While theories have been developed to understand the neural response to stimulation, their predictions have not been thoroughly tested using experimental data. Using a mechanistic coupled oscillator model, we elaborate on two key predictions describing the response to stimulation as a function of the phase and amplitude of ongoing neural activity. To investigate these predictions, we analyze electrocorticogram recordings from a previously conducted study in parkinsonian rats and extract the corresponding phase and amplitude response curves. We demonstrate that the amplitude response to stimulation is strongly correlated to the derivative of the phase response ($\rho > 0.8$) in all animals except one, thereby validating a key model prediction. The second prediction postulates that the stimulation becomes ineffective when the network synchrony is high, a trend that appeared missing in the data. Our analysis explains this discrepancy by showing that the neural populations in parkinsonian rats did not reach the level of synchrony for which the theory would predict ineffective stimulation. Our results highlight the potential of fine-tuning stimulation paradigms informed by mathematical models that consider both the ongoing phase and amplitude of the targeted neural oscillation.

Key words: brain oscillations; Kuramoto model; Parkinson's disease; phase-locked; stimulation

---

Significance Statement

This study validates a mathematical model of coupled oscillators in predicting the response of neural activity to stimulation for the first time. Our findings also offer further insights beyond this validation. For instance, the demonstrated correlation between phase response and amplitude response is indeed a key theoretical concept within a subset of mathematical models. This prediction can bring about clinical implications in terms of predictive power for manipulation of neural activity. Additionally, while phase dependence in modulation has been previously studied, we propose a general framework for studying amplitude dependence as well. Lastly, our study reconciles the seemingly contradictory views of pathological hypersynchrony and theoretical low synchrony in Parkinson's disease.

Introduction

Application of brain stimulation techniques has gained momentum over the past few decades owing to their therapeutic potential (Lozano et al., 2019; Krauss et al., 2021). Neural

Copyright © 2025 Mirkhani et al.

oscillations can act as anchor points in modulation of brain circuitry (Bergmann and Hartwigsen, 2021; Sullivan et al., 2021). The association of particular network oscillations with different brain functions, as well as their implications in many neurological and psychiatric disorders, renders them suitable targets for stimulation (Strüber and Herrmann, 2020; Oswal et al., 2021; Basu et al., 2023; Zaaimi et al., 2023). Successful manipulation of neural oscillations for the desired outcome requires clear answers to where, how, and when to stimulate (Polanía et al., 2018; Cagnan et al., 2019; Hollunder et al., 2022). The first question has been extensively researched to identify the target site based on the engaged networks (Drobisz and Damborská, 2019; Li et al., 2020; Figee and Mayberg, 2021; Kübler et al., 2021; Rajamani et al., 2024). To address how and when stimulation should be applied, a variety of closed-loop strategies have been proposed, where features of the ongoing oscillation serve as feedback (Brittain et al., 2013; Scangos et al., 2021; Mondragón-González et al., 2024).

Among closed-loop techniques, phase-locked stimulation has shown promise in achieving a controlled modulation (Brittain et al., 2013; Cagnan et al., 2017; Mansouri et al., 2018; Krugliakova et al., 2024). In this approach, stimulation pulses are triggered at certain phases of the ongoing oscillatory activity. Neuromodulation and plasticity effects obtained through precise timing of the pulses have been shown to be bidirectional (Huerta and Lisman, 1995; Zanos et al., 2018; Nieuwhof et al., 2022; Li et al., 2023). This feature not only results in higher control and in turn more efficient stimulation policies but may also explain the heterogeneity observed in many open-loop stimulation paradigms. Additionally, due to interactions between different brain rhythms through mechanisms such as phase amplitude coupling, phase-based modulation of an activity can bring about cross-frequency changes (Salimpour et al., 2022; Duchet and Bogacz, 2024).

Despite growing interest in phase-locked stimulation, two main bottlenecks of completely different natures have hindered further application of this strategy. Firstly, real-time tracking of signal properties at the resolution of milliseconds is challenging. Thanks to recent technological advancements and developed algorithms, several studies have demonstrated the implementation of such fast brain-machine interactions in rodents (Siegle and Wilson, 2014; McNamara et al., 2022), nonhuman primates (Escobar Sanabria et al., 2020; Zaaimi et al., 2023), and humans (Reis et al., 2021; Gordon et al., 2022). Secondly, theoretical understanding of how the state of a network oscillation at the stimulation time, i.e., its phase and amplitude, modulates the response remains incomplete, often resulting in an extensive search during stimulation sessions for the desired effect. There have been several theoretical studies proposing optimal closed-loop policies (Holt et al., 2016; Popovych et al., 2017; Weerasinghe et al., 2019, 2021). However, the predictions made by these studies have not been thoroughly validated with experimental data, severely limiting their applicability.

Mathematical models based on coupled oscillators are suitable candidates for bridging this gap due to their ability to replicate neural oscillations (Velazquez et al., 2015; Guevara Erra et al., 2017; Weerasinghe et al., 2021; Sermon et al., 2024). The Kuramoto model, in particular, offers a great advantage for studying phase-locked stimulation by adopting a phase-based description of neural oscillators (Brown et al., 2004; Acebrón et al., 2005). Hence, network dynamics can be explicitly modeled as a function of individual oscillators' phases, which evolve over time based on their natural frequencies and mutual interactions. This model expresses the collective behavior of oscillators in terms of a mean phase and network synchrony, directly proportional to the amplitude of oscillations (Weerasinghe et al., 2019). Given the phase (Cagnan et al., 2017; McNamara et al., 2022) and amplitude (Weerasinghe et al., 2019; Hebron et al., 2024) dependence of stimulation effects, predicting the network response as a function of these two quantities potentially provides clinically translatable predictive power, especially for patients suffering from Parkinson's disease (PD) or essential tremor (ET; Meidahl et al., 2017; Frey et al., 2022). The gained insight could also pave the way for combining phase-locked stimulation with adaptive stimulation—a strategy based on ongoing amplitude (Tinkhauser et al., 2017; Smyth et al., 2023)—merging the best of both approaches.

Here, we aim to expand on the predictions introduced in Weerasinghe et al. (2019) and test them using previously collected experimental data from McNamara et al. (2022). We review the predictions derived from the reduced (mean-field) Kuramoto model regarding the role of ongoing oscillations' phase and amplitude in response to stimulation. Each theoretical prediction is tested separately against the electrocorticogram

measurements of parkinsonian rats subjected to phase-locked stimulation. Phase-wise, we first demonstrate a strong correlation between the amplitude response curve (ARC) and the derivative of the phase response curve (PRC). Regarding the role of amplitude, we show using the full model that the largest effects can be attained by stimulation at intermediate values of network synchrony. Below this peak, where most brain networks operate, the response is characterized by a slight drop and relatively stronger amplification compared with suppression. Taken together, these findings bridge the gap between theory and experiments, unveiling an opportunity to manipulate neural activities in the desired direction more reliably.

Materials and Methods

To investigate the effects of stimulation, we introduce our modeling approach and describe the previously collected dataset used to validate the model's predictions. We also detail the techniques employed to link theory and experiments.

Modeling framework. The Kuramoto model of coupled oscillators was used to model the oscillations arising from the activity of a neuronal population. In this framework, the network dynamics are described through phases that reflect self-sustained oscillations of weakly coupled oscillators (Strogatz, 2000). We employed such a network model to analyze how external stimulation affects the network activity of a population. In this context, neurons or neural microcircuits with periodic behavior can be regarded as oscillators that interact with each other (Weerasinghe et al., 2019), collectively giving rise to the network activity often recorded in experiments as local field potentials (LFPs) or ECoG oscillations (Fig. 1A,B; Breakspear, 2017; Bick et al., 2020).

To assess the impact of external stimulation on these networks, one must make an assumption about how individual oscillators respond to stimulation. Neurons may vary in their phase response depending on their type and various regulating factors (Fink et al., 2013; Goldberg et al., 2013; Phillips et al., 2020). We adopted the classic case compatible with the Hodgkin–Huxley model, where a spiking neuron exhibits a biphasic response featuring both phase delay and advance regions (Goldberg et al., 2013). This response behavior, known as type II, has been observed experimentally (Netoff et al., 2005; Akam et al., 2012) and characterized by a slow-down region after the spiking during the refractory period and a speed-up region closely before the spiking (Fig. 1C; Smeal et al., 2010). We used $Z(\theta) = -\sin\theta$ as a simple phase response function that satisfies these conditions (Fig. 1D,E).

The Hodgkin–Huxley model used to demonstrate the concept of a biphasic phase response was developed using the original conductance values and rate functions (Hodgkin and Huxley, 1952). The effect of stimulation was incorporated as an injected square pulse of current with a width of 50 μs. Numerical simulations were performed in MATLAB using the Euler method with 0.01 ms time steps.

Full Kuramoto model. The dynamics of a finite number of coupled oscillators with noise are governed by Sakaguchi (1988):

$$\dot{\theta}_i = \omega_i$$
$$+ K/N \sum_{j}^{N} \sin(\theta_j - \theta_i) + \xi_i + I(t)Z(\theta_i) \quad \text{for } i = 1, \ldots, N.$$

$$(1)$$

This set of differential equations describes how the phase of each oscillator, θ_i, evolves in time while interacting with other oscillators through a global coupling constant K and being subject to external stimulation $I(t)$ and independent white noise ξ_i:

$$\langle \xi_i(t) \rangle = 0 , \quad \langle \xi_i(t)\xi_j(t') \rangle = 2D\delta(t - t')\delta_{ij}, \quad (2)$$

where D represents noise intensity. δ and δ_{ij} are the delta Dirac and Kronecker delta functions, respectively.
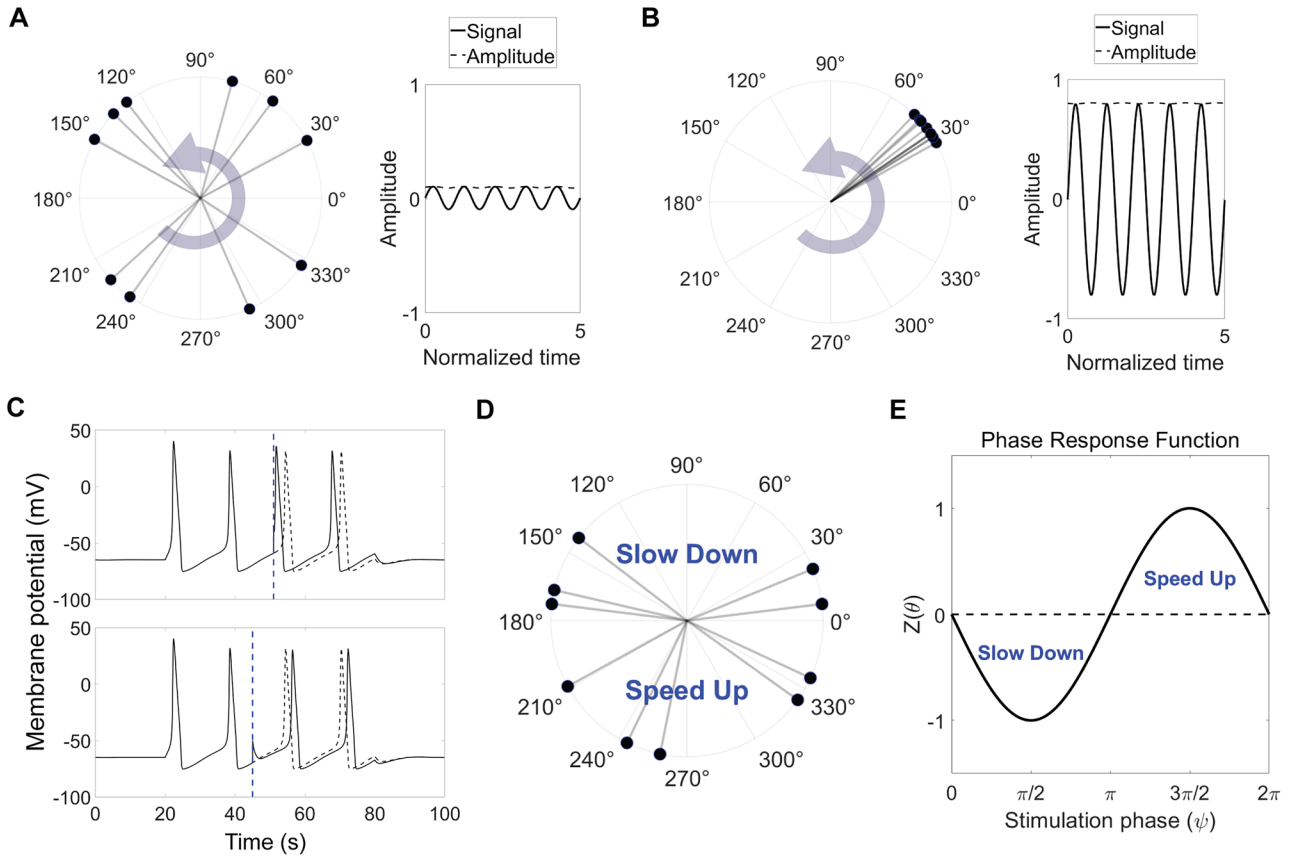
Figure 1. The Kuramoto model of coupled oscillators to model oscillatory neural activity. ***A***, ***B***, Snapshots of two example sets of coupled oscillators with low (***A***) and high (***B***) synchrony levels. Dispersed oscillators result in small oscillatory signal and therefore low amplitude, while packed oscillators represent large oscillation amplitude. ***C***, Shift of spiking in a Hodgkin Huxley model as a result of external stimulation. Depending on the stimulation time with respect to the spiking cycle it can lead to phase advance (top) or delay (bottom). The dashed lines represent the spiking behavior in the absence of stimulation. ***D***, Schematics of the biphasic response behavior incorporated in the model. ***E***, Phase response function of an individual oscillator (here, $-\sin\theta$).

To investigate macroscopic properties of these networks, an order parameter is defined as follows:

$$r = \frac{1}{N}\sum_j^N e^{i\theta_j} = \rho e^{i\psi}, \tag{3}$$

which describes the network activity in terms of the level of synchrony, ρ (ranging from 0 to 1), and the mean phase, ψ. It can be shown that the experimentally measured oscillation amplitude is proportional to the value of synchrony (Weerasinghe et al., 2019).

Numerical simulations were conducted in MATLAB using the Euler–Maruyama method with a time step 0.5 ms to discretize the system in time. We verified convergence of the numerics for this timestep value. The natural frequencies of oscillators were randomly sampled from a Cauchy distribution with a mean frequency of ω_0 and a width of γ. To simulate phase-locked stimulation, conditions similar to those in McNamara et al. (2022) were applied. In each stimulation block, a target phase was chosen, and a pulse was delivered when the calculated mean phase crossed this target and >80% of a beta cycle had elapsed since the previous pulse.

Reduced Kuramoto model. In the limit of an infinite number of oscillators and under certain assumptions regarding the distribution of natural frequencies, the collective behavior of the network can be described in a simpler way solely by the time evolution of the order parameter (Ott and Antonsen, 2008; Bick et al., 2020). The dynamics of the system, assuming $Z(\theta) = -\sin\theta$, are reduced to two differential equations governing amplitude (synchrony ρ) and mean phase ψ of the network:

$$\frac{d\rho}{dt} = -\gamma\rho + \frac{K\rho}{2}(1-\rho^2) + \frac{I(t)}{2}(1-\rho^2)\cos(\psi), \tag{4}$$

$$\frac{d\psi}{dt} = \omega_0 - \frac{I(t)}{2\rho}(1+\rho^2)\sin(\psi), \tag{5}$$

where γ represents the width of the natural frequency distribution that is centered around ω_0. The last terms in the amplitude and phase equations represent the instantaneous population ARC and PRC, respectively. The ARC represents changes in amplitude as a function of the stimulation phase, and the PRC quantifies variations in the mean phase with respect to the stimulation phase.

In the absence of noise, such networks would reach a steady-state condition with fixed values of ρ. However, in real networks, the oscillation amplitude fluctuates due to finite size effects, noise, and changes in coupling resulting from synaptic plasticity. Nonetheless, the reduced model can be seen as a phenomenological platform that provides intuitions and preliminary predictions. Accordingly, we employed this model as the basis for generating predictions, which were then further refined using the full model to partially capture the missing effects in the reduced model.

ECoG recording from parkinsonian rats. In order to test the validity of the theoretical predictions, we used electrocorticogram (EcoG) recordings collected from rats in McNamara et al. (2022). In this study, in brief, rat models of PD were created through unilateral lesions of the dopaminergic neurons in substantia nigra, resulting in pathologically elevated beta activity in the cortico-basal ganglia network. Stimulating electrodes were then implanted in the globus pallidus (GPe), and activity was recorded using ECoG. Using a real-time implementation of the phase tracking algorithm "Oscilltrack" (Sharott and McNamara, 2022), each subject underwent phase-locked stimulation at eight equally spaced target phases based on the ongoing beta signal. Each trial was targeted at a specific phase and consisted of 10–14 stimulation blocks, each lasting 20 s and separated by 5 s off-epochs where no stimulation was applied (Fig. 2A). Full details are presented in McNamara et al. (2022).
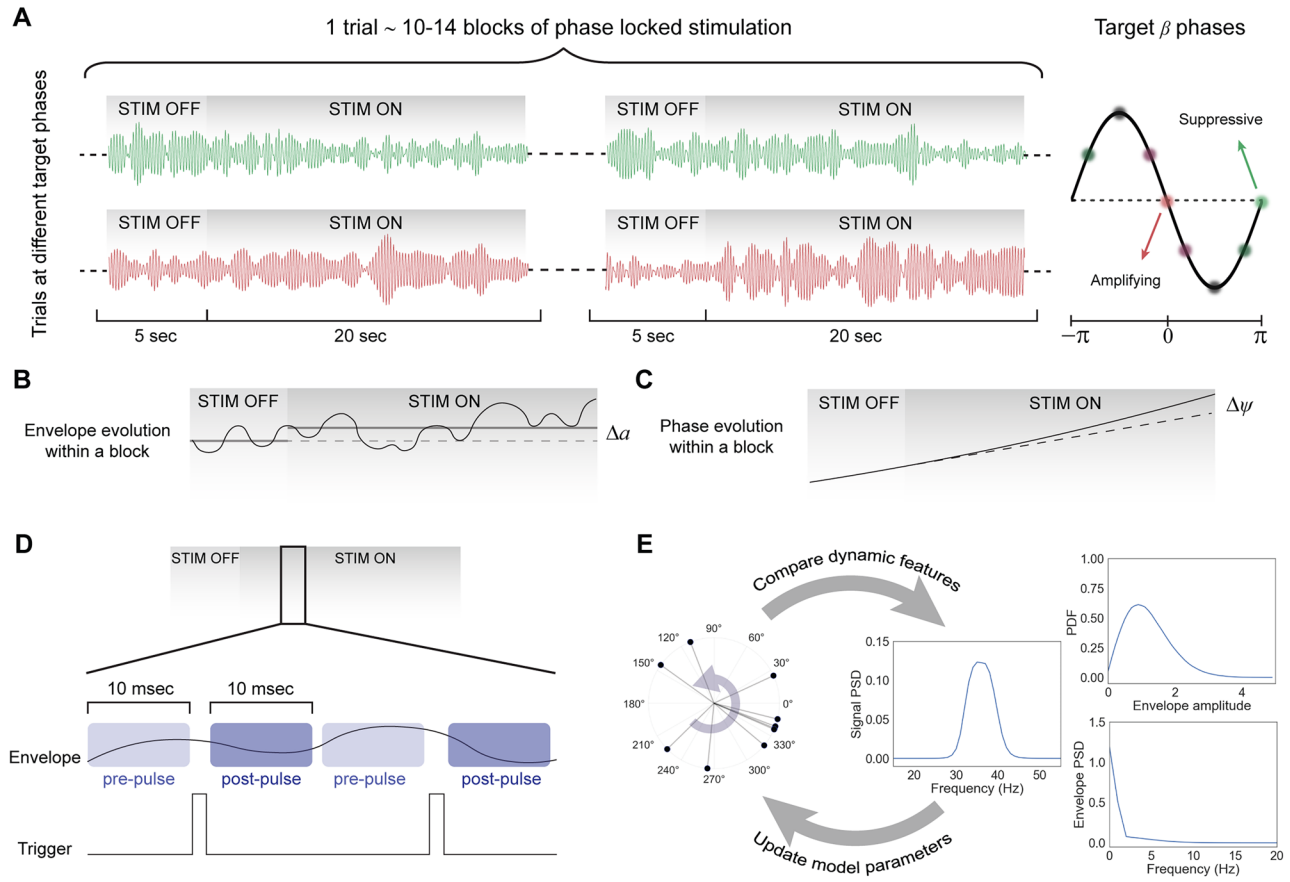
Figure 2. Analysis of experimental data for testing theoretical predictions. ***A***, Summary of phase-locked experimental trials conducted in parkinsonian rats in McNamara et al. (2022). Each trial targeted a certain phase and was divided into 10–14 blocks. Two example signals, one representing stimulation at a suppressing phase (green) and one at an amplifying phase (red) are shown. ***B***, Schematic of block-based quantification of the phase response. ***C***, Schematic of block-based quantification of the amplitude response. ***D***, Schematic of pulse-based quantification of the amplitude response. ***E***, Model fitting algorithm flowchart. Dynamic features of the subject-specific experimental signal were fed into an optimization solver which updates model parameters to minimize the difference between the model and experimental signals.

ECoG recordings were obtained at a sampling rate of 20 kHz. Stimulation artifacts were initially removed by interpolating the signal from the start of the electrical impulse to 1.5 ms after. The resulting signal was then downsampled to 2 kHz using an anti-aliasing filter. A fourth-order bandpass Butterworth filter was subsequently applied to the downsampled signal. The Hilbert transform was then used on the filtered signal to extract the envelope amplitude and phase of the beta oscillations.

Experimental response curves. The primary approach to extract the experimental ARC and PRC was the block-based method, in which the average behavior of the network during each 20 s on-epoch was compared with the preceding 5 s off-epoch. More specifically, for the block-based ARC, the average Hilbert amplitude, $\bar{a}$, of the signal in each epoch was calculated, and the difference represented the amplitude change at the corresponding phase (Cagnan et al., 2017; Duchet et al., 2020; Fig. 2B). Evaluating this change for all target phases enabled us to reconstruct the experimental (block-based) ARC for each animal:

$$\text{ARC}_b = \overline{a_{\text{on}}} - \overline{a_{\text{off}}}. \tag{6}$$

To calculate the block-based PRC, phase trajectory in the 5 s off-epoch was used to fit a linear model for the evolution of the unwrapped phase. Using this model, the expected phase of the system under no stimulation at the end of the 20 s epoch, $\hat{\psi}$, could be estimated. The difference between this estimated unwrapped phase in the absence of stimulation and the actual unwrapped phase, ψ, as a result of the stimulation was then normalized by the number of pulses (N_{pulse}) in the

on-epoch (Fig. 2C). This normalized change was calculated for all target phases, similar to the ARC, to establish the (block-based) PRC for each animal:

$$\text{PRC}_b = \frac{\hat{\psi} - \psi}{N_{\text{pulse}}}. \tag{7}$$

Considering the different sites for stimulation (GPe) and recording (cortex), as well as variability across animals, all curves were phase-aligned based on the most suppressive phase for the purpose of group analysis. To examine the relationship between the response curves, the derivative of the PRC with respect to phase was computed using central differencing.

When quantifying the size of amplitude change under different oscillation amplitudes, the method above averages oscillations over a relatively long period compared with the beta cycle's time scale. To capture more transient changes in the amplitude, we also employed a pulse-based approach. In this technique, the average amplitude within 10 ms before and after each pulse was used to establish the amplitude response as a function of the pre-pulse amplitude (Fig. 2D).

A custom MATLAB script was developed to process the experimental recordings and extract the response curves. Statistical tests and additional data visualizations were carried out using Python-based packages. Pearson's correlation coefficients (R) were calculated to assess the relationship between the ARC and the PRC derivative. Statistical significance of phase dependence in individual ARCs and PRCs was examined using one-way analysis of variance (ANOVA). The relationship between the correlation strength R and the resulting p value from ANOVA was also quantified using the Spearman correlation coefficient (r_s).

Model fitting. To test the prediction based on oscillation amplitude, it was necessary to estimate the network parameters that could reproduce relevant features of the ECoG recordings used for this study. An optimization-based model fitting algorithm was developed in MATLAB to fit the finite Kuramoto model to individual subjects. The algorithm received three dynamic features of the signal (Duchet et al., 2020): power spectrum density (PSD) of the signal, probability density function (PDF) of the envelope amplitude, and PSD of the envelope amplitude (Fig. 2E). These features embed the statistics of the signal intensity along with the temporal variations of both the signal and its amplitude (Sermon et al., 2023). It then employed MATLAB's surrogate optimizer (surrogateopt) with batch update interval 1 to minimize the following error:

$$f = \frac{1}{3}\left(\begin{array}{c} \frac{\sum (\mathrm{PSD}_{\mathrm{Data}} - \mathrm{PSD}_{\mathrm{Model}})^2}{\sum (\mathrm{PSD}_{\mathrm{Data}} - \overline{\mathrm{PSD}_{\mathrm{Data}}})^2} + \frac{\sum (\mathrm{envPDF}_{\mathrm{Data}} - \mathrm{envPDF}_{\mathrm{Model}})^2}{\sum (\mathrm{envPDF}_{\mathrm{Data}} - \overline{\mathrm{envPDF}_{\mathrm{Data}}})^2} \\ + \frac{\sum (\mathrm{envPSD}_{\mathrm{Data}} - \mathrm{envPSD}_{\mathrm{Model}})^2}{\sum (\mathrm{envPSD}_{\mathrm{Data}} - \overline{\mathrm{envPSD}_{\mathrm{Data}}})^2} \end{array} \right).$$

(8)

Given the different scale of the measured values and the model network activity, both experimental and simulated signals were z-scored to ensure comparability. PSDs were calculated using Welch's method with frequency resolution of 1 Hz (1 s window length) and 50 % overlap. The optimization output provided values for four network parameters: mean frequency ω_0, width of the distribution γ, coupling constant K, and standard deviation of the noise σ. The maximum number of function evaluations for the surrogate optimization was set to 500. Network simulations at each optimization step were carried out with N = 200 oscillators which were randomly sampled from a Cauchy distribution with the mean ω_0 and width γ. Each set of parameters was simulated 10 times to account for different realizations of noise, and the dynamic features from the resulting signals were averaged to calculate the optimization error.

A parameter recovery study was also performed using synthetic data to investigate whether the values obtained from the fitting procedure for individual parameters are separately identifiable with respect to network behavior. This series of simulations and optimizations were performed with fewer oscillators ($N = 50$) and lower frequency resolution for PSDs to reduce computational cost while still capturing the model's generalizable features.

Results

The state of simple oscillatory systems can be summarized by their phase and amplitude (Fig. 3A). Hence, a clinically relevant predictive power may arise from studying the response to stimulation as a function of these two quantities tracked from signals of interest (e.g., tremor in ET or beta in PD). We first introduce the predictions made by the reduced model regarding the phase and amplitude dependence of the response to stimulation. We then examine the correlation between the PRC and ARC in the data from parkinsonian rats. Finally, we compare amplitude dependence in the experimental response with simulations of the best-fitting Kuramoto models.

Predictions from the reduced model

First, we focused on the phase dependence of the response behavior (Fig. 3B). Given a specific phase response function for individual oscillators, the reduced model predicted that the population PRC, which represents the phase response of the network, mirrors the form of the individual oscillators' response function (Weerasinghe et al., 2019). More importantly, the amplitude response of the population summarized by the ARC will be negatively correlated with the derivative of the PRC. To develop an intuition about this prediction, two extreme scenarios of maximum suppression and maximum amplification can be helpful. In the former case, when stimulating the network at the mean

phase of π, the trailing oscillators are in the "slow down" region of their cycle while the leading ones have entered the "speed up" regime (Fig. 3B, left inset). As a result, stimulation enlarges the gap between oscillators, causing a more desynchronized system. Conversely, in the maximum amplification scenario, stimulating at the mean phase of 0 causes leading and trailing oscillators to experience opposite effects, making them more tightly packed and thus synchronized (Fig. 3B, right inset). Hence, the maximum suppression and amplification correspond to phases where the absolute slope of the PRC is the largest.

Next, we sought to predict the network response in terms of amplitude dependence. In the reduced model, the last term of Equation 4 $\left(\frac{1}{2}(1-\rho^2)\cos(\psi)\right)$ describes the instantaneous effect of a stimulation impulse, and the scaling factor of this term $\left(\frac{1}{2}(1-\rho^2)\right)$ is plotted in Figure 3C. This plot illustrates that the attainable absolute change in amplitude from stimulation drops continuously as a function of synchrony in the network. In other words, the theory suggests that stimulation should have the greatest effect when applied at low oscillation amplitudes and becomes less effective at large amplitudes. An intuition for this prediction can be obtained by looking at two ends of the synchrony spectrum. Any change in network synchrony requires differential effects of stimulation on the oscillators which leads to an increased or decreased gap between them. In a network with low synchrony, the high dispersion among oscillators allows for the maximum attainable change as a result of stimulation (Fig. 3C, left inset), whereas in a highly synchronized system, all oscillators experience nearly the same change, leading to minimal impact on the collective synchrony (Fig. 3C, right inset).

Examining Equation 4 for amplitude in the reduced model, the last term represents the combined effect of phase and amplitude which can be visualized as a 3D surface (Fig. 3D). For a more detailed assessment of the model's predictions, we tested each component separately using the experimental data.

Correlation between the PRC derivative and ARC

To test the theoretical predictions regarding ARC and PRC, we extracted the corresponding curves from the animal data. Analysis of changes in beta power as a function of target phase in McNamara et al. (2022) revealed nearly antiphase maximum amplification and suppression in all animals. This general trend suggests that $Z(\theta) = -\sin\theta$ can be viewed as a reasonable assumption for phase response function of individual oscillators (Eq. 1). Nevertheless, ARC and PRC curves for each animal enabled a more comprehensive analysis of the predictions. The block-based method, described above, was employed to calculate the phase and amplitude changes in the high-beta activity as a function of the phase of stimulation. The average PRC, pooled across all animals, exhibited the previously described "slow down" and "speed up" regions for the population activity (Fig. 4A). The corresponding ARC also confirmed antiphase maximum suppression and amplification with smooth transitions in between (Fig. 4B). More importantly, the core prediction of the model, which posits a correlation between ARC and PRC derivative, was examined by establishing the derivative curve calculated through central differencing (Fig. 4B). Comparing ARC and PRC derivative revealed a negative correlation, in agreement with the model's prediction.

To further quantify this correlation and its variability across animals, we examined the phase and amplitude responses for 13 individual animals at each of the eight target phases (individual response curves available in Extended Data Fig. 4-1). The data across all animals and phases showed a tight distribution around
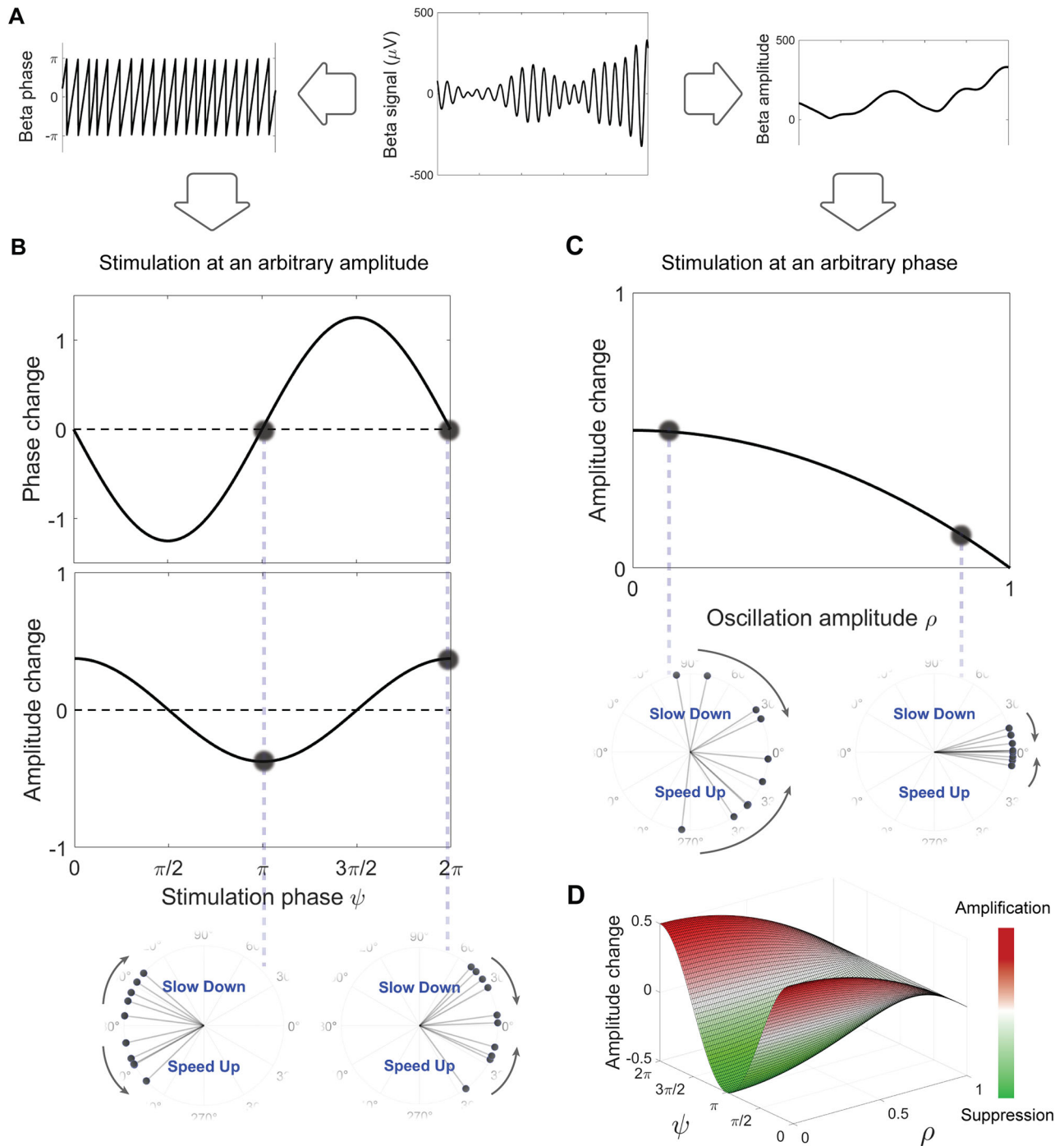
Figure 3. Theoretical predictions of the network response by the Kuramoto model. **A**, Phase and amplitude as the main signal properties. Predictions are based on the network's state in terms of these properties. **B**, Model-based phase dependence of the network response. ARC follows the negative derivative of PRC. Two oscillators' snapshots depict extreme cases of maximum suppression (left) and maximum amplification (right). **C**, Model-based amplitude dependence of the absolute change. Two oscillators' snapshots illustrate stimulation-induced changes in networks with high (left) and low (right) synchrony. **D**, Combined effect of signal's phase and amplitude on the amplitude response.

a line with a negative slope, resulting in a high correlation coefficient ($R = 0.84$) which underscored the validity of the predicted relationship (Fig. 4C; individual correlations available in Extended Data Fig. 4-2). To assess how reliably the amplitude response can be predicted given a specific PRC, the relationship between the correlation strength, R, and the presence of an effect of phase in the PRC was explored. The latter was represented by the p value from the statistical tests where lower values indicate significant phase dependence in the PRC. Plotting these values for different

subjects revealed an interesting trend regarding variability across animals (Fig. 4D). All subjects with statistically significant PRCs exhibited a strong correlation with their amplitude response ($R > 0.8$). Notably, the phase response of the only subject lacking this correlation did not reach the significance threshold. Additionally, subjects with a higher effect of phase tended to show stronger correlations ($r_s = -0.71, p = 6.7 \times 10^{-3}$). These results suggest that when certain model assumptions are met—specifically, when phase dependence is present in the response—a tight
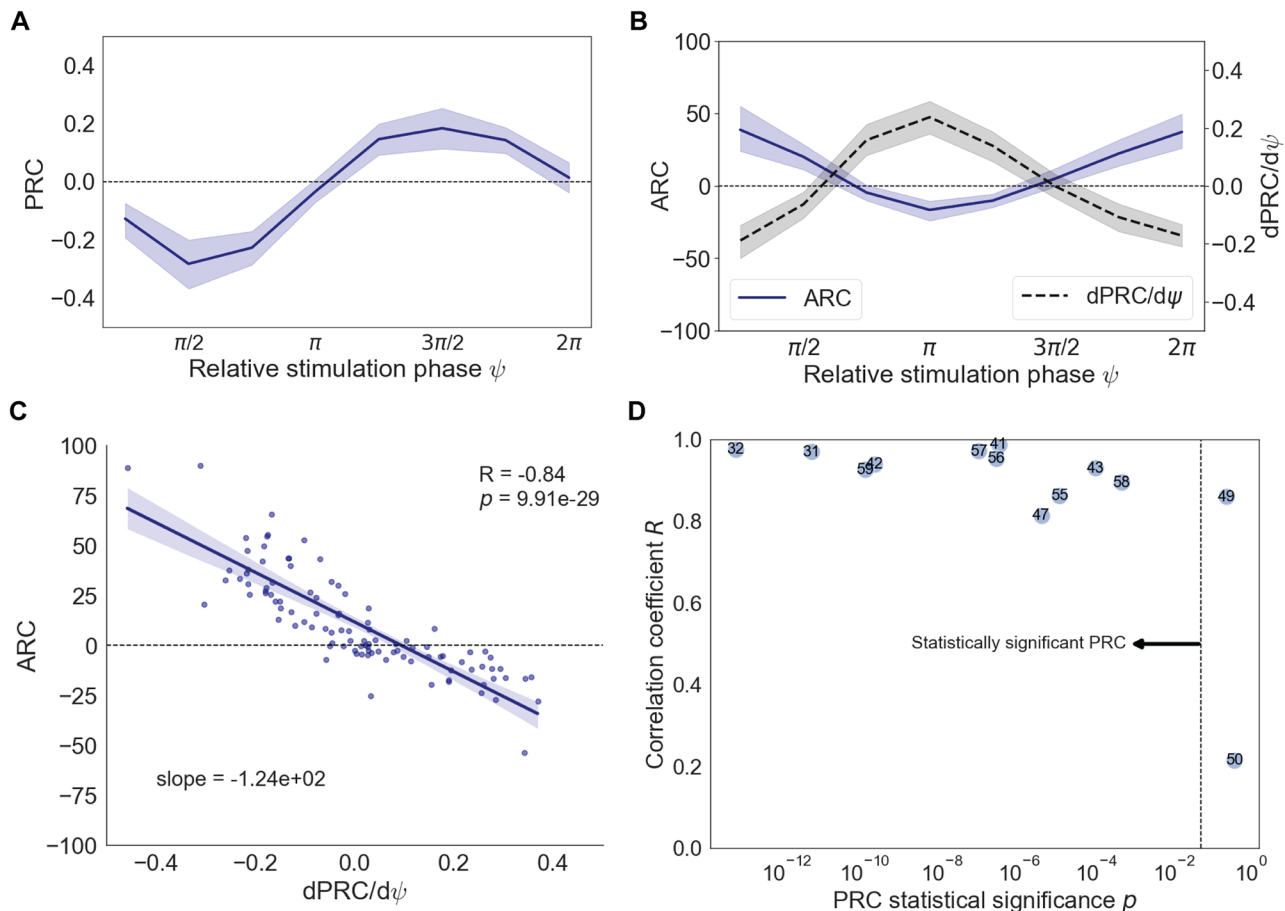
Figure 4. Experimentally validated relationship between ARC and PRC. **A**, Average PRC pooled across all animals. The average response exhibits phase advance and delay for the population activity. **B**, Average ARC (solid line) and PRC derivative (dashed line) pooled across all animals. The average amplitude response in rats is negatively correlated with the derivative of the phase response. Individual response curves are presented in Extended Data Figure 4-1. **C**, ARC as a function of PRC derivative for 13 animals and eight target phases. Individual correlations are presented in Extended Data Figure 4-2. **D**, Relationship between the correlation coefficient and the significance of phase dependence within animals. Subjects (represented by circles labelled with their corresponding numbers) with more statistically significant phase dependence tend to have a stronger correlation between ARC and PRC derivative.

correlation between ARC and PRC derivative may yield clinical insights when evaluating stimulation outcomes.

Contributing factors in amplitude modulation of the response
Following the study of phase dependence, we proceeded with analyzing how the network response is influenced by the ongoing oscillation amplitude. The previously described prediction on the dependence of stimulation effects on the ongoing amplitude (Fig. 3C) was derived from the instantaneous effect of stimulation, i.e., the effect was defined as the difference between amplitude of oscillations just after and just before the pulse. However, to understand longer-term effects, one needs to also consider the dynamics of the system between the pulses. The changes in the oscillation amplitude in the model are described by Equation 4. It states that the amplitude ρ is not only influenced by the stimulation term but also depends on the coupling K and the distribution width γ, which together determine how amplitude evolves in subsequent time steps. In other words, it is not possible to study the longer-term response as a function of amplitude without considering the intrinsic network parameters. In addition, oscillation amplitude is naturally bounded by the minimum and maximum levels of synchrony ($0 < \rho < 1$).

To develop an intuition about the interaction of these contributing forces in amplitude modulation, a seesaw analogy can be useful (Fig. 5A). Each position of a seesaw corresponds to a

specific balance between two opposing forces: one pushing the system toward synchrony and the other causing desynchronization. Within the Kuramoto framework, intrinsic noise D and width γ of the natural frequency distribution, along with external stimulation at phases around the mid-ascending part of the cycle (specific to these experiments), tend to reduce the synchrony of the network, tipping the balance toward lower ρ values (Fig. 5A, top). On the contrary, coupling K in the system and antiphase stimulation—here occuring around the mid-descending part—shift the balance in favor of higher ρ values by enhancing the network synchrony (Fig. 5A, top). Furthermore, analogous to a real seesaw that is constrained at both ends, there are lower and upper bounds on how the force imbalance is reflected in the network (Fig. 5A, bottom).

As mentioned earlier, the introduced Kuramoto model's term for absolute change as a function of oscillation amplitude highlights only the stimulation-induced instantaneous changes in the time evolution of amplitude (Fig. 5B, top), without taking into account network dynamics influenced by intrinsic parameters. The reduced model offers an initial insight into the interaction of these contributing factors. In asynchronous networks (Fig. 5B, left inset), relatively high stimulation-induced perturbations are partially offset by network's tendency to return to its steady state with a low synchrony during the intervals between the pulses. As the network begins transitioning to a partially
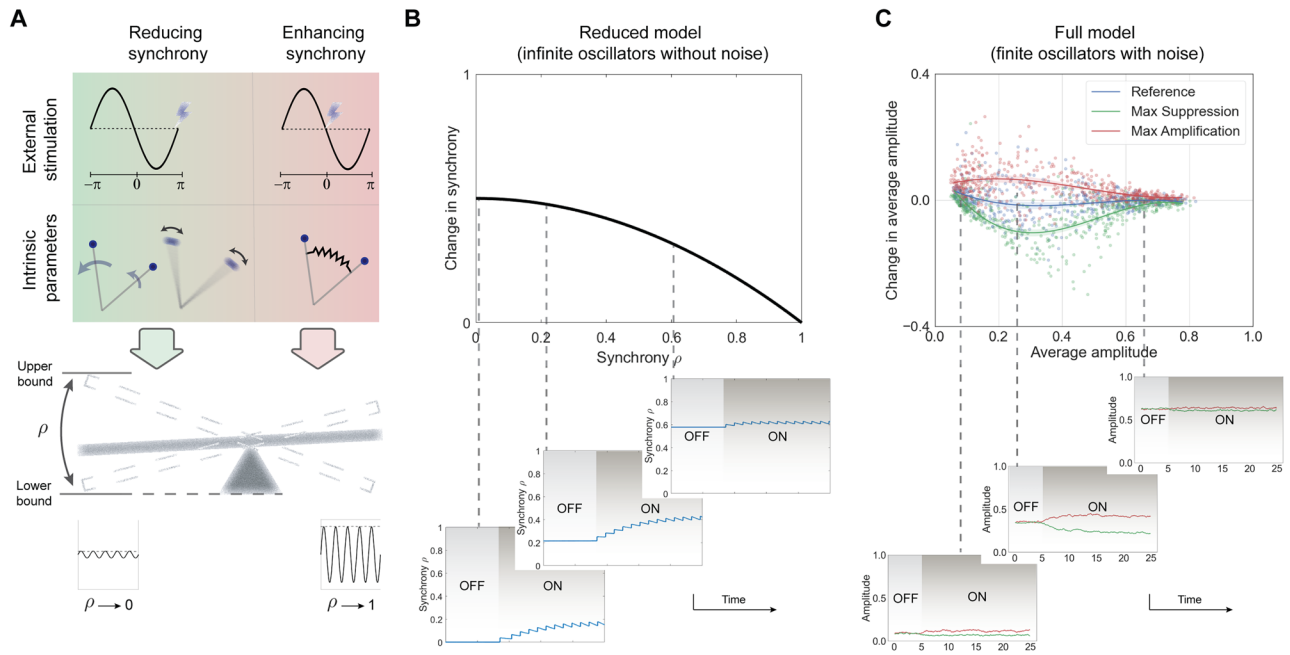
Figure 5. Contributing factors in amplitude modulation of the network response. **A**, A seesaw analogy of a network with two opposing forces and natural upper and lower bounds. External stimulation interacts with intrinsic parameters to determine the synchrony level in a constrained system. **B**, Stimulation-induced instantaneous disturbance as a function of oscillation amplitude. Three examples of synchrony evolution in the reduced model, each representing different steady-state synchrony levels. The extent of change in network synchrony as a result of stimulation depends on the size of the induced disturbance as well as network tendencies at that specific amplitude. Variations of such tendencies can be visualized by the network's characteristic curve presented in Extended Data Figure 5-1. **C**, Simulated block-based change in oscillation amplitude as a function of amplitude prior to stimulation in the full model. Three instances of amplitude evolution within a block illustrate the combined effect of stimulation-induced disturbance, intrinsic network tendencies, and synchrony boundaries.

synchronized state (Fig. 5B, middle inset), a slight decrease in the effect of individual stimulation pulses emerges, but the network is notably more susceptible to changes, reflected in a smaller decay between pulses, which translates into larger shifts in average network synchrony. Lastly, under substantial levels of synchrony (Fig. 5B, right inset), not only is the stimulation effect diminished, but the network again shows a strong tendency to maintain its steady state, leading to smaller net changes in synchrony. Such variations in network tendencies could be better understood by looking at its characteristic curve (Extended Data Fig. 5-1).

To further characterize the absolute change as a function of amplitude and link the model's prediction with the experimental data, changes of oscillation amplitude within similar stimulation blocks were simulated (Fig. 5C, top). The size of impulse was adjusted to match the observed change in beta power in experiments. These simulations were performed using the finite model with stochastic oscillators, and curves corresponding to no stimulation, most suppressive, and most amplifying phases were generated. The combined effects of external stimulation and intrinsic parameters constrained by bounds on both ends were consistent with the above descriptions. The relative weight of each contributing factor at different synchrony levels can be better understood by examining the time evolution of amplitude across three distinct levels of synchrony (Fig. 5C, bottom). In a highly noisy/low coupling network, only the amplifying phase caused a small upward shift in amplitude, as the already low amplitude could not be significantly reduced by stimulation at the suppressing phase (Fig. 5C, left inset). Under intermediate levels of coupling, far from both bounds of synchrony, a two-sided stimulation effect emerged in the response (Fig. 5C, middle inset) which then disappeared under asymptotically high levels of coupling due to the small instantaneous effect of stimulation (Fig. 5C, right inset).

Amplitude dependence of the response in parkinsonian rats
Having refined the prediction for the magnitude of the stimulation effect as a function of synchrony level, we aimed to test it by extracting the corresponding response behavior from the rat data. As outlined in the Materials and Methods section, the oscillation amplitude in the model represents a normalized amplitude corresponding to the level of synchrony. Therefore, to compare experimental curves with theoretical predictions, one needs to first estimate the network synchrony corresponding to the measured ECoG. The model fitting algorithm was employed to determine the subject-specific network parameters ω_0, γ, K, D. A series of parameter recovery studies using synthetic data revealed that while individual parameters could not be reliably recovered (Extended Data Fig. 6-1), the resulting network synchrony derived from each set of parameters was recovered with reasonable confidence (Fig. 6A). As a result, rather than focusing on exact parameter values from the fitting output, the corresponding network synchrony has been reported which indeed is more directly relevant to the theoretical prediction. The fitting was performed to replicate three key dynamic features of the signal for each animal (Fig. 6B).

Results of the model fitting implied that underlying networks producing the measured signals may possess very low sustained synchrony across all animals (Fig. 6C). To highlight that different combinations of network parameters can lead to the same oscillating behavior, reflected by the synchrony level, the fitting algorithm was run multiple times for each subject. Although output parameter values varied within each subject, all combinations consistently represented similar levels of network synchrony (Extended Data Fig. 6-2). The resulting model networks produced beta oscillations similar to those observed in the experiments (Fig. 6D).
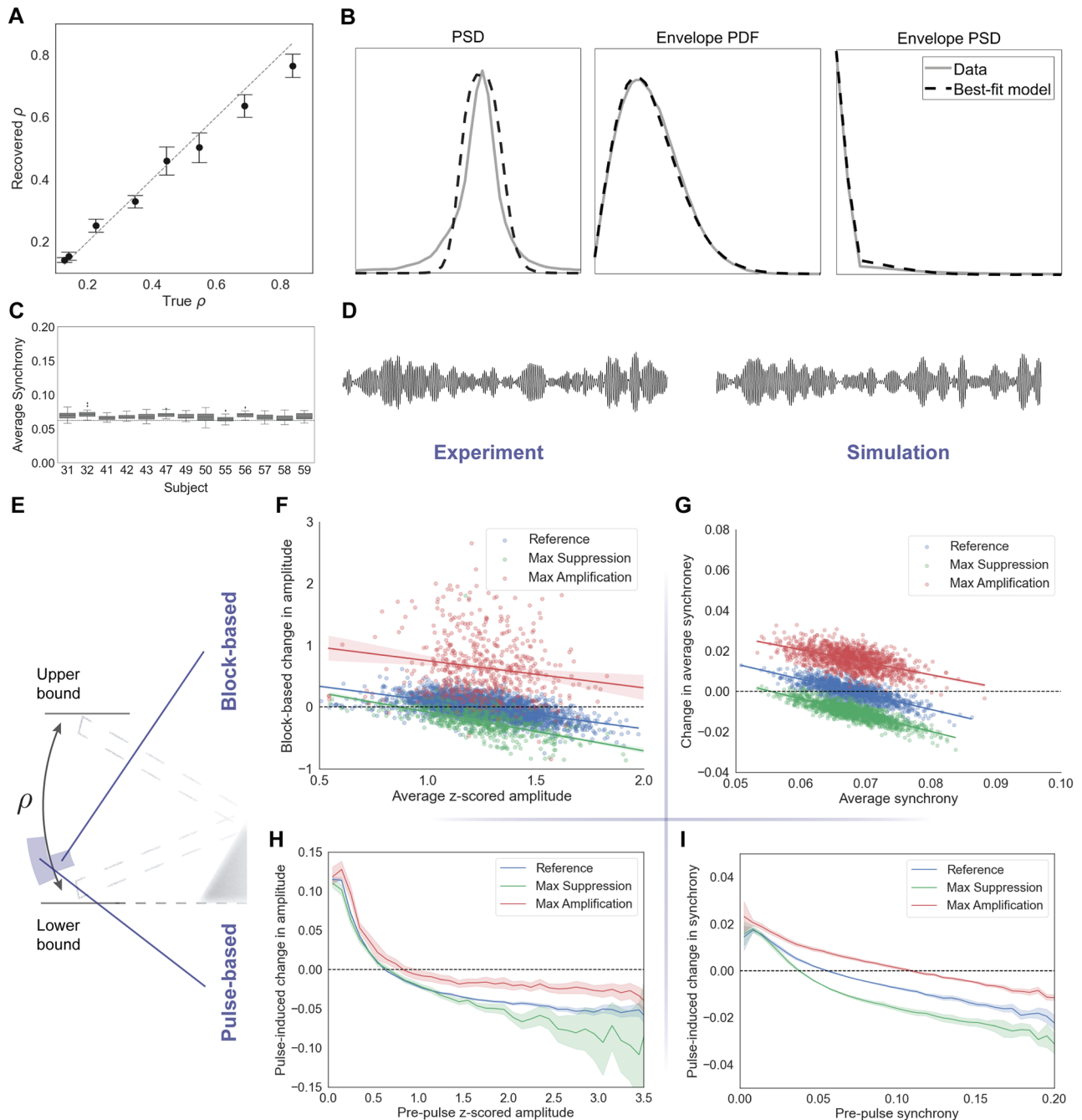
Figure 6. Network response dependence on oscillation amplitude. *A*, Parameter recovery using synthetic data. The model successfully recovers network synchrony from a set of simulated network activities. The recovery results for individual parameters are shown in Extended Data Figure 6-1. *B*, Results of the fitted dynamic features of the signal for an example animal. The power spectral density (PSD) of the signal and its amplitude, along with the probability density function (PDF) of the amplitude, were used to find the best-fitting parameters. *C*, Extracted mean synchrony for different subjects obtained by fitting the Kuramoto model to experimental recordings. The dashed line represents the mean synchrony when desynchronizing factors approach infinity. Details of the fitting for each subject are provided in Extended Data Figure 6-2. *D*, Example epochs of experimental recordings compared with simulated activity generated by the best-fit model. *E*, The relevant range of synchrony in the seesaw analogy. Block-based and pulse-based analyses provide different windows into the network synchrony. *F*, *G*, Block-based changes in amplitude as a function of pre-stimulation amplitude, demonstrating stronger amplification compared with suppression in this regime. *H*, *I*, Pulse-based changes in amplitude as a function of pre-pulse amplitude, revealing a drop in effect size at lower ends of the synchrony range through this quantification method. The reference-subtracted curves for both block-based and pulse-based approaches are presented in Extended Data Figure 6-3.

Next, having identified the synchrony range of interest, we investigated the experimental data under two synchrony windows (block-based vs pulse-based variations) to assess whether the experimental responses aligned with the response of a model operating in that regime (Fig. 6E). As demonstrated in the previous section, low-synchrony networks are predicted to generally exhibit a higher propensity for amplification compared with

suppression (Fig. 5C). By closely examining the blocks in the experiments, the amplitude change as a function of average amplitude prior to the stimulation epoch was obtained under three conditions: reference (no stimulation applied) plus the two phases achieving the highest amplification and highest suppression (Fig. 6F). At a given state, the inherent noise and finite number of oscillators caused a regression to the mean in the

absence of stimulation. The model's response, based on best-fit parameters, aligned with the experimental curves (Fig. 6G). The reference-subtracted regression lines reflected a significant increase in the stimulation effect during the suppressive phase, along with a more subtle, nonsignificant increase for amplification, and an overall more pronounced amplification in this regime (Extended Data Fig. 6-3A).

Lastly, recognizing that using averaged amplitudes over on- and off-epochs narrows the analyzed synchrony window (higher and lower synchrony values are averaged out), similar amplitude dependence curves were also derived based on individual stimulation pulses instead of blocks. This approach accounts for a wider range of momentary synchrony levels that the network experiences. It is worth noting that, while this approach uses smaller windows to calculate changes in amplitude, it still combines stimulation-induced instantaneous effects with peristimulus restoration governed by intrinsic parameters. The experimental pulse-based curves generally exhibited similar trends to the block-based ones, except even smaller changes at the lower end and a peaked trend for the amplification (Fig. 6H). This is consistent with the insight from the previous section that the averaged amplitude change (Fig. 5C, top) exhibits a small dip at the low end of synchrony in contrast to the instantaneous effect of pulses (Fig. 5B, top). These differences were again in agreement with the curves extracted from the best-fit models (Fig. 6I). To visualize the net effects of stimulation, the corresponding reference line could be subtracted from the amplification and suppression lines (Extended Data Fig. 6-3B).

Discussion

In this study, we elaborated on the predictions of a mathematical model based on coupled oscillators regarding the effects of phase-locked stimulation on a population activity. The model put forth predictions on how a neuronal population would respond to stimulation based on its current state in terms of phase and level of synchrony. We utilized a previously collected dataset from the study of phase-locked stimulation in rat models of PD to test those predictions.

For phase dependence, the prediction implied that the shape of ARC would follow the negative of the derivative of PRC, and all except one animal exhibited response behaviors consistent with the model's prediction. This key relationship, validated for the first time in this study, has been investigated previously with different models. Using the Wilson–Cowan model, it has been demonstrated (Duchet et al., 2020) that the phase shift between the ARC and PRC converges to $\pi/2$ in the linearized model. The phase shift was however larger than $\pi/2$ in the nonlinear Wilson–Cowan model and in some of the data from patients with ET. The predictive feature of the PRC derivative was also discussed in Wilson and Moehlis (2014); Wilson et al. (2015) through a noisy oscillators model, and in Holt et al. (2016) with a network of conductance-based neurons. On the other hand, several studies (Escobar Sanabria et al., 2020; Zaaimi et al., 2023; Hebron et al., 2024) have adopted mathematical frameworks to explain the phase-dependent response to stimulation. Findings of these studies have been generally consistent with the explicit relationship between the ARC and PRC discussed here which is derived from a phenomenological model. In addition, when evaluating the effect of phase, it must be kept in mind that perfect phase tracking in practice is not feasible, especially at low amplitudes due to a lower signal-to-noise ratio. Consequently, quantifying the effect of phase based on the higher amplitude portions of the signal may provide a clearer

perspective. Alternatively, collecting more data can help mitigate this issue by averaging out the variations caused by imperfect tracking, which was the case for the data used in this study. Overall, our results support the proposal that a prior estimate of the PRC [such as measurements conducted for cortical (Stiefel et al., 2008), subthalamic (Farries and Wilson, 2012), or pallidal neurons (Goldberg et al., 2013)] may be a useful tool for determining the suppressing or amplifying phase for closed-loop DBS without a full search of the parameter space (Holt et al., 2016). This approach could provide valuable guidance for defining optimal stimulation parameters in clinical settings.

Amplitude dependence is a relatively unexplored aspect of the network response. Focusing solely on the instantaneous effects of stimulation, the theory suggests that stimulation should become ineffective at high network synchrony. However, the amplitude dependence was demonstrated to be more complex as other contributing factors such as network's tendencies and bounds interact with stimulation-induced changes. These interactions would lead to a decay in the effect size of stimulation at both ends of the synchrony range. Moreover, distinct characteristic behaviors may emerge when amplifying oscillatory activity compared with its suppression, as exemplified by the stronger amplification observed in this study. This highlights the significance of determining the synchrony levels of the target network beforehand if the goal is to optimize stimulation efficiency based on ongoing amplitude. This could explain some of the observed differences in suppressing pathological activity in patients with PD compared with those with ET (Brittain et al., 2013; Schreglmann et al., 2021). We proposed here that fitting the Kuramoto model to individual recordings could provide subject-specific models, enabling tailored stimulation paradigms according to the subject and network under study. It is also important to note that the size of electrical impulses and the attainable modulation in clinical settings, which was simulated here to achieve comparable changes in power, could shift the location and intensity of peaks in the amplitude dependence of the response. The first-order trend, which is a general drop of the effect size with increasing amplitude, has been reported in several studies (Wang et al., 2022; Hebron et al., 2024) and agrees with the intuition that the stronger the synchrony of a network, the harder it is to disrupt.

Beta oscillations in PD are considered an exemplar of pathological hypersynchrony. Therefore, it could be considered surprising that the stimulation effect did not drop at higher amplitudes in parkinsonian rats. Importantly, however, high synchronization in the Kuramoto model represents almost complete alignment of individual oscillators (Fig. 3C, right). In the parkinsonian brain, beta synchronization between neurons is massively elevated compared with healthy animals, where there is very little oscillatory synchronization (Raz et al., 2001; Mallet et al., 2008a,b); However, if oscillators in the model represent individual neurons or ensembles of neurons in the basal ganglia circuit, these pathological levels of synchronization do not approach the levels of hypersynchronization in the model. For example, in the subthalamic nucleus of parkinsonian patients, the maximum proportion of individual neurons that oscillate at beta frequency and/or are synchronized with cortical beta oscillations is ~60%, with a mean of 20–30% (Sharott et al., 2014, 2018). In the context of developing novel approaches for DBS in PD, this suggests that even highly pathophysiological levels of beta synchronization remain in the region where they remain responsive to modulation by phase-dependent stimulation. It remains to be seen

whether this is also the case for pathophysiological activities with higher levels of synchronization, such as epilepsy.

It is worth highlighting that, besides phase and amplitude, another commonly studied aspect of response prediction is the frequency of oscillations and their entrainment to external rhythmic stimulation—a phenomenon described by Arnold tongues. However, our analysis focused on modulating a narrow band—specifically, beta oscillations—in an adaptive manner. Although an average stimulation frequency can be defined in such closed-loop approaches, establishing a direct connection is challenging because only one band is targeted and the stimulation strength does not vary significantly.

With regard to limitations, although the model seems to capture the mean synchrony for subject-specific models that reproduce the ECoG recordings, it falls short of replicating the variability of oscillation amplitude observed in the animals, as seen when comparing the x-axes in Figure 6F–I. This limitation could potentially be addressed by allowing for changes in the coupling as a result of synaptic plasticity and/or using a more generalized coupled oscillators model where oscillators are allowed to vary in their amplitudes. Additionally, while the model also makes predictions about specific stimulation phases that lead to suppression or amplification given a specific response function $Z(\theta)$, only the correlation between ARC and the PRC derivative was tested due to the separate stimulation and recording sites in the experiments. Applying the developed framework on experimental data where sensing and stimulation has been conducted through the same electrode may facilitate further validation of the model's prediction. Moreover, the focus here was placed on beta rhythms originated from basal ganglia which feature a bursty characteristic with very low sustained synchrony. Testing the model through other brain rhythms and networks will provide a more comprehensive image of the effects of phase-locked stimulation. Lastly, alternative methods of measuring the experimental ARC and PRC could lead to slightly different outcomes which is why analytical methods alone may not be sufficient to estimate network synchronies.

In terms of the mechanistic explanation of the response to stimulation, it is worth noting that the proposed mechanism—delayed and accelerated cycles of oscillators—can be applied at different levels of abstraction, depending on the specific neural activity. While regular-spiking neurons may represent the simplest interpretation of individual oscillators in some localized signals, other oscillatory drives could account for broader network signals. Consequently, pinpointing the exact mechanism and realization of these oscillators hinges on the scale of the measured signal and may require recordings at multiple scales.

In summary, this study aimed to bridge the gap between theory and experiments by validating relatively straightforward yet powerful predictions. Such mechanistic understanding of the effects of stimulation could complement model-free approaches like machine learning techniques to design more effective stimulation policies. The findings of this study highlight the significance of pinpointing the right time for stimulation, providing clinically translatable insights for optimizing closed-loop strategies.

Data Availability

No new data were generated in this study. The experimental data used here is available at http://dx.doi.org/10.5287/bodleian:9omadD7Pp. The developed codes for mathematical modeling and computational analysis would be made available on https://github.com/Bogacz-Group upon publication.

References

Acebrón JA, Bonilla LL, Pérez Vicente CJ, Ritort F, Spigler R (2005) The Kuramoto model: a simple paradigm for synchronization phenomena. Rev Mod Phys 77:137–185.

Akam T, Oren I, Mantoan L, Ferenczi E, Kullmann DM (2012) Oscillatory dynamics in the hippocampus support dentate gyrus–CA3 coupling. Nat Neurosci 15:763–768.

Basu I, et al. (2023) Closed-loop enhancement and neural decoding of cognitive control in humans. Nat Biomed Eng 7:576–588.

Bergmann TO, Hartwigsen G (2021) Inferring causality from noninvasive brain stimulation in cognitive neuroscience. J Cogn Neurosci 33:195–225.

Bick C, Goodfellow M, Laing CR, Martens EA (2020) Understanding the dynamics of biological and neural oscillator networks through exact mean-field reductions: a review. J Math Neurosci 10:9.

Breakspear M (2017) Dynamic models of large-scale brain activity. Nat Neurosci 20:340–352.

Brittain J-S, Probert-Smith P, Aziz TZ, Brown P (2013) Tremor suppression by rhythmic transcranial current stimulation. Curr Biol 23:436–440.

Brown E, Moehlis J, Holmes P (2004) On the phase reduction and response dynamics of neural oscillator populations. Neural Comput 16:673–715.

Cagnan H, et al. (2017) Stimulating at the right time: phase-specific deep brain stimulation. Brain 140:132–145.

Cagnan H, Denison T, McIntyre C, Brown P (2019) Emerging technologies for improved deep brain stimulation. Nat Biotechnol 37:1024–1033.

Drobisz D, Damborská A (2019) Deep brain stimulation targets for treating depression. Behav Brain Res 359:266–273.

Duchet B, Bogacz R (2024) How to design optimal brain stimulation to modulate phase-amplitude coupling? J Neural Eng 21:046006.

Duchet B, Weerasinghe G, Cagnan H, Brown P, Bick C, Bogacz R (2020) Phase-dependence of response curves to deep brain stimulation and their relationship: from essential tremor patient data to a Wilson–Cowan model. J Math Neurosci 10:4.

Escobar Sanabria D, Johnson LA, Yu Y, Busby Z, Nebeck S, Zhang J, Harel N, Johnson MD, Molnar GF, Vitek JL (2020) Real-time suppression and amplification of frequency-specific neural activity using stimulation evoked oscillations. Brain Stimul 13:1732–1742.

Farries MA, Wilson CJ (2012) Phase response curves of subthalamic neurons measured with synaptic input and current injection. J Neurophysiol 108:1822–1837.

Figee M, Mayberg H (2021) The future of personalized brain stimulation. Nat Med 27:196–197.

Fink CG, Murphy GG, Zochowski M, Booth V (2013) A dynamical role for acetylcholine in synaptic renormalization. PLoS Comput Biol 9:e1002939.

Frey J, Cagle J, Johnson KA, Wong JK, Hilliard JD, Butson CR, Okun MS, de Hemptinne C (2022) Past, present, and future of deep brain stimulation: hardware, software, imaging, physiology and novel approaches. Front Neurol 13:825178.

Goldberg JA, Atherton JF, Surmeier DJ (2013) Spectral reconstruction of phase response curves reveals the synchronization properties of mouse globus pallidus neurons. J Neurophysiol 110:2497–2506.

Gordon PC, Belardinelli P, Stenroos M, Ziemann U, Zrenner C (2022) Prefrontal theta phase-dependent rTMS-induced plasticity of cortical and behavioral responses in human cortex. Brain Stimul 15:391–402.

Guevara Erra R, Perez Velazquez JL, Rosenblum M (2017) Neural synchronization from the perspective of non-linear dynamics. Front Comput Neurosci 11:98.

Hebron H, Lugli B, Dimitrova R, Jaramillo V, Yeh LR, Rhodes E, Grossman N, Dijk D-J, Violante IR (2024) A closed-loop auditory stimulation approach selectively modulates alpha oscillations and sleep onset dynamics in humans. PLoS Biol 22:e3002651.

Hodgkin AL, Huxley AF (1952) A quantitative description of membrane current and its application to conduction and excitation in nerve. J Physiol 117:500–544.

Hollunder B, Rajamani N, Siddiqi SH, Finke C, Kühn AA, Mayberg HS, Fox MD, Neudorfer C, Horn A (2022) Toward personalized medicine in connectomic deep brain stimulation. Prog Neurobiol 210:102211.

Holt AB, Wilson D, Shinn M, Moehlis J, Netoff TI (2016) Phasic burst stimulation: a closed-loop approach to tuning deep brain stimulation parameters for Parkinson's disease. PLoS Comput Biol 12:e1005011.

Huerta PT, Lisman JE (1995) Bidirectional synaptic plasticity induced by a single burst during cholinergic theta oscillation in CA1 in vitro. Neuron 15:1053–1063.

Krauss JK, et al. (2021) Technology of deep brain stimulation: current status and future directions. Nat Rev Neurol 17:75–87.

Krugliakova E, et al. (2024) Exploring the local field potential signal from the subthalamic nucleus for phase-targeted auditory stimulation in Parkinson's disease. Brain Stimul 17:769–779.

Kübler D, Kroneberg D, Al-Fatly B, Schneider G-H, Ewert S, van Riesen C, Gruber D, Ebersbach G, Kühn AA (2021) Determining an efficient deep brain stimulation target in essential tremor - cohort study and review of the literature. Parkinsonism Relat Disord 89:54–62.

Li N, et al. (2020) A unified connectomic target for deep brain stimulation in obsessive-compulsive disorder. Nat Commun 11:3364.

Li Q, et al. (2023) Reinstating olfactory bulb-derived limbic gamma oscillations alleviates depression-like behavioral deficits in rodents. Neuron 111:2065–2075.e5.

Lozano AM, et al. (2019) Deep brain stimulation: current challenges and future directions. Nat Rev Neurol 15:148–160.

Mallet N, Pogosyan A, Márton LF, Bolam JP, Brown P, Magill PJ (2008a) Parkinsonian beta oscillations in the external globus pallidus and their relationship with subthalamic nucleus activity. J Neurosci 28:14245–14258.

Mallet N, Pogosyan A, Sharott A, Csicsvari J, Bolam JP, Brown P, Magill PJ (2008b) Disrupted dopamine transmission and the emergence of exaggerated beta oscillations in subthalamic nucleus and cerebral cortex. J Neurosci 28:4795–4806.

Mansouri F, Fettes P, Schulze L, Giacobbe P, Zariffa J, Downar J (2018) A real-time phase-locking system for non-invasive brain stimulation. Front Neurosci 12:877.

McNamara CG, Rothwell M, Sharott A (2022) Stable, interactive modulation of neuronal oscillations produced through brain-machine equilibrium. Cell Rep 41:111616.

Meidahl AC, Tinkhauser G, Herz DM, Cagnan H, Debarros J, Brown P (2017) Adaptive deep brain stimulation for movement disorders: the long road to clinical therapy. Mov Disord 32:810–819.

Mondragón-González SL, Schreiweis C, Burguière E (2024) Closed-loop recruitment of striatal interneurons prevents compulsive-like grooming behaviors. Nat Neurosci 27:1148–1156.

Netoff TI, Acker CD, Bettencourt JC, White JA (2005) Beyond two-cell networks: experimental measurement of neuronal responses to multiple synaptic inputs. J Comput Neurosci 18:287–295.

Nieuwhof F, Toni I, Buijink AWG, van Rootselaar A-F, van de Warrenburg BPC, Helmich RC (2022) Phase-locked transcranial electrical brain stimulation for tremor suppression in dystonic tremor syndromes. Clin Neurophysiol 140:239–250.

Oswal A, et al. (2021) Neural signatures of hyperdirect pathway activity in Parkinson's disease. Nat Commun 12:5185.

Ott E, Antonsen TM (2008) Low dimensional behavior of large systems of globally coupled oscillators. Chaos 18:037113.

Phillips RS, Rosner I, Gittis AH, Rubin JE (2020) The effects of chloride dynamics on substantia nigra pars reticulata responses to pallidal and striatal inputs. Elife 9:e55592.

Polanía R, Nitsche MA, Ruff CC (2018) Studying and modifying brain function with non-invasive brain stimulation. Nat Neurosci 21:174–187.

Popovych OV, Lysyansky B, Rosenblum M, Pikovsky A, Tass PA (2017) Pulsatile desynchronizing delayed feedback for closed-loop deep brain stimulation. PLoS One 12:e0173363.

Rajamani N, et al. (2024) Deep brain stimulation of symptom-specific networks in Parkinson's disease. Nat Commun 15:4662.

Raz A, Frechter-Mazar V, Feingold A, Abeles M, Vaadia E, Bergman H (2001) Activity of pallidal and striatal tonically active neurons is correlated in MPTP-treated monkeys but not in normal monkeys. J Neurosci 21:RC128.

Reis C, Arruda BS, Pogosyan A, Brown P, Cagnan H (2021) Essential tremor amplitude modulation by median nerve stimulation. Sci Rep 11:17720.

Sakaguchi H (1988) Cooperative phenomena in coupled oscillator systems under external fields. Prog Theor Phys 79:39–46.

Salimpour Y, Mills KA, Hwang BY, Anderson WS (2022) Phase- targeted stimulation modulates phase-amplitude coupling in the motor cortex of the human brain. Brain Stimul 15:152–163.

Scangos KW, et al. (2021) Closed-loop neuromodulation in an individual with treatment-resistant depression. Nat Med 27:1696–1700.

Schreglmann SR, et al. (2021) Non-invasive suppression of essential tremor via phase-locked disruption of its temporal coherence. Nat Commun 12:363.

Sermon JJ, Olaru M, Ansó J, Cernera S, Little S, Shcherbakova M, Bogacz R, Starr PA, Denison T, Duchet B (2023) Sub-harmonic entrainment of cortical gamma oscillations to deep brain stimulation in Parkinson's disease: model based predictions and validation in three human subjects. Brain Stimul 16:1412–1424.

Sermon JJ, Wiest C, Tan H, Denison T, Duchet B (2024) Evoked resonant neural activity long-term dynamics can be reproduced by a computational model with vesicle depletion. Neurobiol Dis 199:106565.

Sharott A, et al. (2014) Activity parameters of subthalamic nucleus neurons selectively predict motor symptom severity in Parkinson's disease. J Neurosci 34:6273–6285.

Sharott A, et al. (2018) Spatio-temporal dynamics of cortical drive to human subthalamic nucleus neurons in Parkinson's disease. Neurobiol Dis 112:49–62.

Sharott A, McNamara C (2022) OscillTrack – real-time neuronal oscillation tracking for closed-loop stimulation. Available at: http://dx.doi.org/10.5287/bodleian:qa9ngXrzr [Accessed October 16, 2024].

Siegle JH, Wilson MA (2014) Enhancement of encoding and retrieval functions through theta phase-specific manipulation of hippocampus. Elife 3:e03061.

Smeal RM, Ermentrout GB, White JA (2010) Phase-response curves and synchronized neural networks. Philos Trans R Soc Lond B Biol Sci 365:2407–2422.

Smyth C, Anjum MF, Ravi S, Denison T, Starr P, Little S (2023) Adaptive deep brain stimulation for sleep stage targeting in Parkinson's disease. Brain Stimul 16:1292–1296.

Stiefel KM, Gutkin BS, Sejnowski TJ (2008) Cholinergic neuromodulation changes phase response curve shape and type in cortical pyramidal neurons. PLoS One 3:e3947.

Strogatz SH (2000) From Kuramoto to Crawford: exploring the onset of synchronization in populations of coupled oscillators. Physica D 143:1–20.

Strüber D, Herrmann CS (2020) Modulation of gamma oscillations as a possible therapeutic tool for neuropsychiatric diseases: a review and perspective. Int J Psychophysiol 152:15–25.

Sullivan CRP, Olsen S, Widge AS (2021) Deep brain stimulation for psychiatric disorders: from focal brain targets to cognitive networks. Neuroimage 225:117515.

Tinkhauser G, Pogosyan A, Little S, Beudel M, Herz DM, Tan H, Brown P (2017) The modulatory effect of adaptive deep brain stimulation on beta bursts in Parkinson's disease. Brain 140:1053–1067.

Velazquez JLP, Erra RG, Rosenblum M (2015) The epileptic thalamocortical network is a macroscopic self-sustained oscillator: evidence from frequency-locking experiments in rat brains. Sci Rep 5:8423.

Wang J, Deng B, Gao T, Wang J, Liu C (2022) Modulation of cortical oscillations by periodic electrical stimulation is frequency-dependent. Commun Nonlinear Sci Numer Simul 110:106356.

Weerasinghe G, Duchet B, Bick C, Bogacz R (2021) Optimal closed-loop deep brain stimulation using multiple independently controlled contacts. PLoS Comput Biol 17:e1009281.

Weerasinghe G, Duchet B, Cagnan H, Brown P, Bick C, Bogacz R (2019) Predicting the effects of deep brain stimulation using a reduced coupled oscillator model. PLoS Comput Biol 15:e1006575.

Wilson D, Holt AB, Netoff TI, Moehlis J (2015) Optimal entrainment of heterogeneous noisy neurons. Front Neurosci 9:192.

Wilson D, Moehlis J (2014) Locally optimal extracellular stimulation for chaotic desynchronization of neural populations. J Comput Neurosci 37:243–257.

Zaaimi B, et al. (2023) Closed-loop optogenetic control of the dynamics of neural activity in non-human primates. Nat Biomed Eng 7:559–575.

Zanos S, Rembado I, Chen D, Fetz EE (2018) Phase-locked stimulation during cortical beta oscillations produces bidirectional synaptic plasticity in awake monkeys. Curr Biol 28:2515–2526.e4.